Wavelength-size hybrid Si-VO_2 waveguide electroabsorption optical switches and photodetectors

Arash Joushaghani,[1,3] Junho Jeong,[1] Suzanne Paradis,[2] David Alain,[2] J. Stewart Aitchison,[1] and Joyce K. S. Poon[1*]

[1] *Department of Electrical and Computer Engineering, University of Toronto, 10 King's College Road, Toronto, Ontario, M5S 3G4, Canada*
[2] *Defence Research and Development Canada - Valcartier, 2459 Pie-XI Blvd. North, Quebec, Quebec G3J 1X5, Canada*

[3] *arash.joushaghani@utoronto.ca*
**joyce.poon@utoronto.ca*

Abstract: Ultra-compact waveguide electroabsorption optical switches and photodetectors with micron- and sub-micron lengths and compatible with silicon (Si) waveguides are demonstrated using the insulator-metal phase transition of vanadium dioxide (VO_2). A 1 μm long hybrid Si-VO_2 device is shown to achieve a high extinction ratio of 12 dB and a competitive insertion loss of 5 dB over a broad bandwidth of 100 nm near $\lambda = 1550$ nm. The device, operated as a photodetector, can measure optical powers less than 1 μW with a responsivity in excess of 10 A/W. With volumes that are about 100 to 1000 times smaller than today's active Si photonic components, the hybrid Si-VO_2 devices show the feasibility of integrating transition metal oxides on Si photonic platforms for nanoscale electro-optic elements.

© 2015 Optical Society of America

OCIS codes: (350.4238) Nanophotonics; (130.3120) Integrated optics devices; (160.2100) Electro-optical materials.

References and links

1. Q. Xu, B. Schmidt, S. Pradhan, and M. Lipson, "Micrometre-scale silicon electro-optic modulator," Nature **435**, 325–327 (2005).
2. A. Biberman, E. Timurdogan, W. A. Zortman, D. C. Trotter, and M. R. Watts, "Adiabatic microring modulators," Opt. Express **20**, 29223–29236 (2012).
3. A. E.-J. Lim, T.-Y. Liow, F. Qing, N. Duan, L. Ding, M. Yu, G.-Q. Lo, and D.-L. Kwong, "Novel evanescent-coupled germanium electro-absorption modulator featuring monolithic integration with germanium p-i-n photodetector," Opt. Express **19**, 5040–5046 (2011).
4. J. Liu, M. Beals, A. Pomerene, S. Bernardis, R. Sun, J. Cheng, L. C. Kimerling, and J. Michel, "Waveguide-integrated, ultralow-energy GeSi electro-absorption modulators," Nat. Photon. **2**, 433–437 (2008).
5. Y. Tang, H.-W. Chen, S. Jain, J. D. Peters, U. Westergren, and J. E. Bowers, "50 Gb/s hybrid silicon traveling-wave electroabsorption modulator," Opt. Express **19**, 5811–5816 (2011).
6. M. Liu, X. Yin, E. Ulin-Avila, B. Geng, T. Zentgraf, L. Ju, F. Wang, and X. Zhang, "A graphene-based broadband optical modulator," Nature **474**, 64–67 (2011).
7. L. Chen, Q. Xu, M. G. Wood, and R. M. Reano, "Hybrid silicon and lithium niobate electro-optical ring modulator," Optica **1**, 112–118 (2014).
8. V. J. Sorger, D. Lanzillotti-Kimura Norberto, R.-M. Ma, and X. Zhang, "Ultra-compact silicon nanophotonic modulator with broadband response," Nanophotonics **1**, 17—22 (2012).

#228930 - $15.00 USD Received 4 Dec 2014; revised 20 Jan 2015; accepted 23 Jan 2015; published 5 Feb 2015

DRDC-RDDC-2015-P022

9. A. Joushaghani, B. A. Kruger, S. Paradis, D. Alain, J. Stewart Aitchison, and J. K. S. Poon, "Sub-volt broadband hybrid plasmonic-vanadium dioxide switches," Appl. Phys. Lett. **102**, 061101–061101 (2013).
10. R. M. Briggs, I. M. Pryce, and H. A. Atwater, "Compact silicon photonic waveguide modulator based on the vanadium dioxide metal-insulator phase transition," Opt. Express **18**, 11192–11201 (2010).
11. J. D. Ryckman, V. Diez-Blanco, J. Nag, R. E. Marvel, B. K. Choi, R. F. Haglund, and S. M. Weiss, "Photothermal optical modulation of ultra-compact hybrid Si-VO_2 ring resonators," Opt. Express **20**, 13215–13225 (2012).
12. J. D. Ryckman, K. A. Hallman, R. E. Marvel, R. F. Haglund, and S. M. Weiss, "Ultra-compact silicon photonic devices reconfigure by an optically induced semiconductor-to-metal transition," Opt. Express **21**, 10753–10763 (2013).
13. A. Cavalleri, C. Toth, C. W. Siders, J. A. Squier, F. Raksi, P. Forget, and J. C. Kieffer, "Femtosecond structural dynamics in VO_2 during an ultrafast solid-solid phase transition," Phys. Rev. Lett. **87**, 237401 (2001).
14. M. Liu, H. Y. Hwang, H. Tao, A. C. Strikwerda, K. Fan, G. R. Keiser, A. J. Sternbach, K. G. West, S. Kittiwatanakul, J. Lu, S. A. Wolf, F. G. Omenetto, X. Zhang, K. A. Nelson, and R. D. Averitt, "Terahertz-field-induce insulator-to-metal transition in vanadium dioxide metamaterial," Nature **487**, 345–348 (2012).
15. J. Cao, E. Ertekin, V. Srinivasan, W. Fan, S. Huang, H. Zheng, J. W. L. Yim, D. R. Khanal, D. F. Ogletree, J. C. Grossman, and J. Wu, "Strain engineering and one-dimensional organization of metal-insulator domains in single-crystal vanadium dioxide beams," Nat. Nano. **4**, 732–737 (2009).
16. C. N. Berglund and H. J. Guggenheim, "Electronic properties of VO_2 near the semiconductor-metal transition," Phys. Rev. **185**, 1022–1033 (1969).
17. G. Stefanovich, A. Pergament, and D. Stefanovich, "Electrical switching and Mott transition in VO_2," J. of Phys.: Cond. Matt. **12**, 8837 (2000).
18. M. Nakano, K. Shibuya, D. Okuyama, T. Hatano, S. Ono, M. Kawasaki, Y. Iwasa, and Y. Tokura, "Collective bulk carrier delocalization driven by electrostatic surface charge accumulation," Nature **487**, 459–462 (2012).
19. A. Joushaghani, J. Jeong, S. Paradis, D. Alain, J. Stewart Aitchison, and J. K. S. Poon, "Voltage-controlled switching and thermal effects in VO_2 nano-gap junctions," Appl. Phys. Lett. **104**, 221904 (2014).
20. P. Markov, J. D. Ryckman, R. E. Marvel, K. A. Hallman, R. F. Haglund, and S. M. Weiss, "Silicon-VO_2 hybrid electro-optic modulator," in "CLEO: 2013," (Optical Society of America, 2013), p. CTu2F.7.
21. L. A. Sweatlock and K. Diest, "Vanadium dioxide based plasmonic modulators," Opt. Express **20**, 8700–8709 (2012).
22. B. A. Kruger, A. Joushaghani, and J. K. S. Poon, "Design of electrically driven hybrid vanadium dioxide (VO_2) plasmonic switches," Opt. Express **20**, 23598–23609 (2012).
23. Y. Vlasov and S. McNab, "Losses in single-mode silicon-on-insulator strip waveguides and bends," Opt. Express **12**, 1622–1631 (2004).
24. A. Joushaghani, J. Jeong, S. Paradis, D. Alain, J. Stewart Aitchison, and J. K. S. Poon, "Separating the carrier and thermally induced phase transitions in VO_2 microwires," (submitted) (2014).
25. A. Joushaghani, "Micro- and nano-scale optoelectronic devices using vanadium dioxide," Ph.D. thesis, University of Toronto (2014).
26. C. Ye, S. Khan, Z. R. Li, E. Simsek, and V. J. Sorger, "λ-size ITO and graphene-based electro-optic modulators on SOI," IEEE J. Sel. Top. Quant. Electron. **20**, 3400310 (2014).
27. D. Feng, B. J. Luff, and M. Asghari, "Recent advances in manufactured silicon photonics integrated circuits," in "Proc. SPIE," , vol. 8265 (2012), pp. 826507–826507–9.
28. Y. Painchaud, M. Poulin, F. Pelletier, C. Latrasse, J.-F. Gagné, S. Savard, G. Robidoux, M. . Picard, S. Paquet, C. . Davidson, M. Pelletier, M. Cyr, C. Paquet, M. Guy, M. Morsy-Osman, M. Chagnon, and D. V. Plant, "Silicon-based products and solutions," in "Proc. SPIE," , vol. 8988 (2014), pp. 89880L–89880L–14.
29. M. R. Watts, J. Sun, C. DeRose, D. C. Trotter, R. W. Young, and G. N. Nielson, "Adiabatic thermo-optic Mach-Zehnder switch," Opt. Lett. **38**, 733–735 (2013).
30. S. Park, K. Yamada, T. Tsuchizawa, T. Watanabe, H. Shinojima, H. Nishi, R. Kou, and S. Itabashi, "Influenc of carrier lifetime on performance of silicon p-i-n variable optical attenuators fabricated on submicrometer rib waveguides," Opt. Express **18**, 11282–11291 (2010).
31. A. Joushaghani, J. Jeong, S. Paradis, D. Alain, J. Stewart Aitchison, and J. K. S. Poon, "Electronic and thermal effects in the insulator-metal phase transition in VO_2 nano-gap junctions," Appl. Phys. Lett. **105**, 231904 (2014).
32. S. Lysenko, V. Vikhnin, A. Rua, F. Fernandez, and H. Liu, "Critical behavior and size effects in light-induced transition of nanostructured VO_2 films" Phys. Rev. B **82**, 205425 (2010).
33. M. Hada, D. Zhang, A. Casandruc, R. J. D. Miller, Y. Hontani, J. Matsuo, R. E. Marvel, and R. F. Haglund, "Hot electron injection driven phase transitions," Phys. Rev. B **86**, 134101 (2012).
34. K. Appavoo, B. Wang, N. F. Brady, M. Seo, J. Nag, R. P. Prasankumar, D. J. Hilton, S. T. Pantelides, and R. F. Haglund, "Ultrafast phase transition via catastrophic phonon collapse driven by plasmonic hot-electron injection," Nano Lett. **14**, 1127–1133 (2014).
35. Y. Zhang and S. Ramanathan, "Analysis of switching times for thermally driven VO_2 metal-insulator transition nanoscale switching devices," Solid-State Electron. **62**, 161–164 (2011).
36. J. M. Wu and W. E. Chang, "Ultrahigh responsivity and external quantum efficien y of an ultraviolet-light photodetector based on a single VO_2 microwire," ACS Appl. Mater. Interfaces **6**, 14286–14292 (2014).

#228930 - $15.00 USD Received 4 Dec 2014; revised 20 Jan 2015; accepted 23 Jan 2015; published 5 Feb 2015
(C) 2015 OSA

37. G. T. Reed, G. Mashanovich, F. Y. Gardes, and D. J. Thomson, "Silicon optical modulators," Nat. Photon. **4**, 518–526 (2010).
38. D. Thomson, F. Gardes, J.-M. Fedeli, S. Zlatanovic, Y. Hu, B. P. P. Kuo, E. Myslivets, N. Alic, S. Radic, G. Mashanovich, and G. Reed, "50-Gb/s silicon optical modulator," IEEE Photon. Technol. Lett. **24**, 234–236 (2012).

1. Introduction

Shrinking the size of active photonic devices, such as optical switches and modulators, can lower the power consumption and increase the integration density of photonic circuits, but has remained challenging despite much progress in the fiel of nanophotonics. Although high index contrast dielectric or metal-dielectric platforms have reduced the transverse dimensions of active waveguide devices, device lengths remain long due to the weak electro-optic effect in most optical materials. To reduce device sizes, one approach is to use optical microcavities, which restrict the operation wavelengths to narrow-band resonances [1,2]. Another option is to hybridize waveguides with materials that have significant voltage-controllable changes in their optical constants, such as germanium [3] and its composites [4], compound semiconductors [5], graphene [6], lithium niobate [7], indium tin oxide [8], and transition metal oxides including vanadium dioxide (VO_2) [9–12].

Of these materials, VO_2 has the largest change in the optical absorption in the infrared wavelength range due to a reversible insulator-metal phase transition that collapses its electronic bandgap. Vanadium oxides are used for commercial thermal sensors and bolometers, and thus have the potential to be scaled to volume production. The phase transition in VO_2 decreases the resistivity by up to three orders of magnitude and changes the complex refractive index from about $2.9+0.4i$ in the insulating phase to about $2.0+3i$ in the metallic phase at $\lambda = 1550$ nm [9]. The refractive index of VO_2 depends on the material quality and deposition conditions. The values in [9], which are also used in this work, were measured by ellipsometry for our VO_2 samples. The phase transition can be initiated by external stimuli [13–15], such as heating [16], applied electrical field or currents [17–19], and optical absorption [13]. Recent experiments have demonstrated hybrid silicon (Si)-VO_2 waveguides on silicon-on-insulator (SOI) can be switched by substrate heating [10], optical pumping [11,12], or an applied fiel [20]. In these experiments, however, the measured extinction ratios (ERs) were limited to 4 dB, far from the ultimate capability of VO_2.

In this paper, we present ultra-compact, hybrid Si-VO_2 waveguide devices operated as electroabsorption optical switches and photodetectors. The devices were wavelength-size in all three spatial dimensions. As electroabsorption optical switches, the devices exhibited very high extinction ratios, modest insertion losses, and low power consumption. A 1 μm long Si-VO_2 device had an ER of 12 dB and an insertion loss (IL) of 5 dB. To the best of our knowledge, this represents the highest ER-per-length for any electrically controlled waveguide switch or modulator. Owing to the small volume, the power-time constant product figur of merit of the device was more than 10 times smaller than Si switches that use carrier injection in a PIN diode or the thermo-optic effect. The same device operated as a photodetector could measure optical powers less than 1 μW with a responsivity $>$ 10 A/W. In contrast to our earlier demonstration of hybrid VO_2-plasmonic switches in [9], the current result does not rely on a hybrid plasmonic mode and demonstrates smaller device sizes and lower power consumption. The excellent performance of these wavelength-size devices was realized by tailoring the optical modes to the electrical and optical properties of the VO_2 film

#228930 - $15.00 USD Received 4 Dec 2014; revised 20 Jan 2015; accepted 23 Jan 2015; published 5 Feb 2015
(C) 2015 OSA

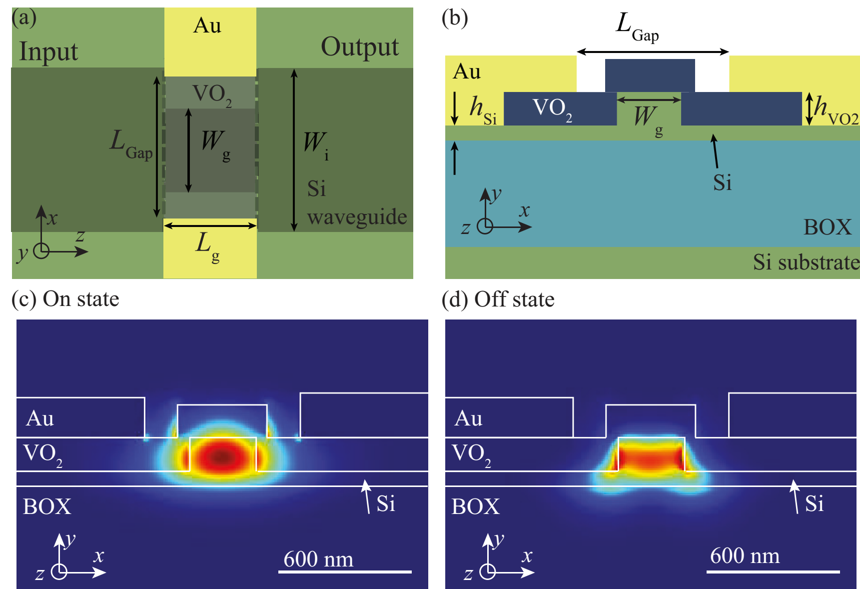

Fig. 1. (a) A schematic of the Si-VO_2 electroabsorption switch. (b) The cross-section of the Si-VO_2 waveguide. The simulated electric fiel intensity of the Si-VO_2 waveguide when the VO_2 was in the (c) insulating and (d) metallic state.

2. Device design

Figure 1(a) shows the device schematic. Si waveguides were define in SOI with a 220 nm thick top-Si layer and a 2 μm thick buried oxide. The input to the Si-VO_2 switch was a Si rib waveguide with a width of W_i and a slab height of h_{Si}. Single-mode strip Si waveguides (not shown in Fig. 1(a)) were connected to the rib waveguides using adiabatic tapers. The cross-section of the hybrid Si-VO_2 waveguide is illustrated in Fig. 1(b). A VO_2 layer with thickness h_{VO2} surrounds a Si rib with a width of W_g and length of L_g. Two gold (Au) pads with a separation of L_{Gap} were used to inject carriers into the VO_2 to induce the insulator-metal phase transition.

To achieve a high ER and minimize IL, the Si-VO_2 waveguide should switch between a pair of modes that have different propagation losses depending on the phase of the VO_2, but have similar effective indices and mode profile as the input/output Si rib waveguides. Thus, optical switching would be due to the propagation through the Si-VO_2 section rather than a change in the input/output coupling losses. Ideally, the Si-VO_2 hybrid mode should have minimal mode overlap with the VO_2 in the ON state, and a maximal mode overlap with the VO_2 in the OFF state. However, the index difference between VO_2 and Si *increases* across the insulator-metal phase transition, so if VO_2 is simply placed atop the Si waveguide, the optical mode becomes more confine in the Si as the absorption of the VO_2 increases. This problem is more severe with the fundamental transverse electric (TE0) mode, which is more confine in the Si than the transverse magnetic (TM) mode. It is possible to confin light in a low-index dielectric, using, for example, plasmonic or slot waveguides [8,9,21,22], but these methods often work only for the TM polarization, which is not preferred for common Si photonic platforms, since the TE0 mode has a lower loss and higher confinemen near 1550 nm [23].

To overcome these challenges, in our design, the VO_2 layer surrounds a narrow Si core region that delocalizes the TE mode, so light is forced into the VO_2 in the metallic state. From

#228930 - $15.00 USD Received 4 Dec 2014; revised 20 Jan 2015; accepted 23 Jan 2015; published 5 Feb 2015
(C) 2015 OSA

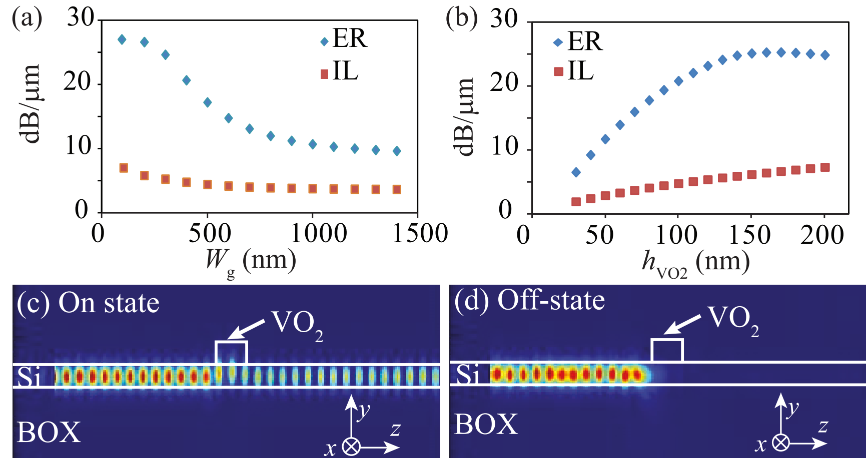

Fig. 2. The computed ER and IL as a function of (a) W_g (for h_{Si} = 70 nm and h_{VO2} = 150 nm) and (b) h_{VO2} (for W_g = 300 nm and h_{Si} = 70 nm). The computed electric fiel intensity along the propagation axis and center of the waveguide when the device is in the (c) ON and (b) OFF state. The device dimensions are W_i = 1.1 μm, W_g = 300 nm, h_{Si} = 70 nm, h_{VO2} = 150 nm, and L_g = 500 nm.

electromagnetic simulations and considering fabrication limitations and electrical contact integration, we chose a design with $W_g = 300$ nm, $h_{Si} = 70$ nm, and $h_{VO2} = 150$ nm, assuming a VO_2 refractive index of $2.9+0.4i$ in the insulating phase and $2.0+3i$ in the metallic phase at $\lambda = 1550$ nm [9]. When VO_2 is in the insulating phase, the designed Si-VO_2 waveguide supports a low-loss, TE mode shown in Fig. 1(c). This hybrid mode has a calculated effective index of $n_{eff} = 2.6$, a propagation loss of 6.1 dBμm^{-1}, and an optimal overlap with the fundamental TE mode of the input Si waveguide with $W_i = 1.1$ μm. When VO_2 is in the metallic state, the waveguide supports a hybridized TE metal-dielectric-metal-like mode that is mainly confine between the VO_2 and Si as shown in Fig. 1(d). This lossy mode has an effective index of $n_{eff} = 2.3$ and a propagation loss of 31.5 dBμm^{-1}. Therefore, using the VO_2 phase transition, the two modes predict a theoretical ER-per-length of 25.5 dBμm^{-1} and IL of 6.1 dBμm^{-1}. Although the per-length loss is high, the device can be kept short (< 1 μm) such that a sufficientl high ER can be achieved with losses comparable to conventional hybrid Si devices. The mode mismatch loss is about 0.3 dB at each interface. The insertion loss of the switch may be reduced at longer wavelengths for which the absorption of VO_2 is lower.

Figure 2(a) shows the computed ER and IL of the hybrid Si-VO_2 switch as a function of the W_g when the VO_2 thickness is $h_{VO2} = 150$ nm and $h_{Si} = 70$ nm. As W_g decreases, the mode overlap with the VO_2 increases, which increases the IL and ER. As $W_g \to 0$, the ER saturates to about 25 dBμm^{-1}. IL and ER decrease as W_g increases, since the light becomes more confine in the Si. Figure 2(b) shows the calculated IL and ER as a function of h_{VO2} for $W_g = 300$ nm and $h_{Si} = 70$ nm. When $h_{VO2} < 150$ nm, the mode overlap with the VO_2 increases as the VO_2 thickness increases, boosting the IL and ER. As h_{VO2} increases beyond 150 nm, the IL continues to increase, but the ER begins to drop due to the finit VO_2 optical penetration depth, which is about 150 nm.

To ensure the complete phase transition in VO_2, the contacts and VO_2 dimensions were designed based on the electrical characteristics of microwires formed in the film [24]. The contacts had a thickness of 200 nm and were separated by a gap, L_{Gap}, of about 700 nm, which was sufficien for the optical scattering from the contacts to be negligible, while maintaining

#228930 - $15.00 USD Received 4 Dec 2014; revised 20 Jan 2015; accepted 23 Jan 2015; published 5 Feb 2015
(C) 2015 OSA

a low switching voltage. Decreasing L_{Gap} increases optical scattering loss, but decreases the switching voltage and power.

Figures 2(c) and 2(d) show the electric fiel intensity along the mid-line of the waveguide computed using three-dimensional finit difference time domain (FDTD) simulations (Lumerical FDTD). The optical input is the TE0 mode of the Si rib waveguide with $W_i = 1.1$ μm and $h_{Si} = 70$ nm. The hybrid Si-VO_2 section has a width of $W_g = 300$ nm and a length of $L_g = 500$ nm. In the ON state, light efficientl transmits through the Si-VO_2 section to result in an IL of < 3.6 dB. In the OFF state, the light is absorbed in the VO_2 layer with minimal reflection

3. Fabrication and measurement setup

The devices were fabricated with a series of aligned electron-beam (e-beam) lithography, deposition, and etching steps [25]. Square alignment markers were firs formed on an SOI substrate using e-beam lithography and lift-off of a 100 nm thick tungsten film The top-Si thickness of the SOI was 220 nm. The Si rib waveguides were formed using a two-step aligned e-beam lithography and reactive ion etching of Si with etch depths of 150 nm and 70 nm. Polycrystalline VO_2 with a thickness of 150 nm was then deposited on the chip using radio-frequency magnetron sputtering at a substrate temperature of 773 K. Deposition at temperatures less than 673 K would be preferred for CMOS compatible backend of line processing. VO_2 regions were define along the Si waveguides using aligned e-beam lithography and dry etching with a mixture of Cl_2, H_2, and Ar. A subsequent e-beam lithography step and wet etching of VO_2 using a dilute solution of MicroChemicals Cr etchant in H_2O in a 1:100 ratio removed the VO_2 residue around the waveguides to reduce the insertion loss. Au contacts were then formed using aligned e-beam lithography, thermal evaporation, and lift-off. More details about the fabrication and VO_2 deposition processes are available in [25]. Figure 3(a) shows the microscope image of a fabricated device with $L_g = 500$ nm, $W_i = 1.1$ μm, $W_g = 350$ nm, and $L_{Gap} = 500$ nm.

To experimentally characterize the devices, continuous wave (CW), linearly polarized light from a tunable laser was coupled into the waveguides using a tapered fibe with a nominal spot size of 3 μm at a wavelength of 1550 nm. The output light was collected using an 40× objective lens, which focused the light either onto an InGaAs infrared camera or into a free-space photodetector. The samples were placed on a temperature controlled stage held at room temperature for these experiments. Tungsten electrical probes contacted the Au pads on the chip. A current was applied to the Si-VO_2 device using a precision sourcemeter. A resistor was connected in series with the device under test for the current regulation.

4. Electroabsorption optical switches

4.1. DC characteristics

Figure 3(b) shows the current vs. applied voltage, V_{App}, characteristics of two devices, one with $L_g = 500$ nm and $L_{Gap} = 500$ nm and another with $L_g = 1$ μm and $L_{Gap} = 1$ μm. Each device was in series with an external resistance of $R_L = 2$ kΩ. The insulator-metal phase transition occured at a voltage, $V_{I \to M}$, which resulted in a sharp increase in the current. In our VO_2 films the current filamen that initiated the phase transition should be about 1 μm wide, which would be sufficien to cover the entire VO_2 section [24]. Figure 3(c) shows the normalized optical transmission of the devices as a function of V_{App}. The transmission decreased dramatically after the insulator-metal phase transition. An ER of 12.3 ± 1.5 dB was achieved for the 1 μm long device. The device IL was determined by comparing the transmission against an equivalent waveguide without the hybrid Si-VO_2 section to be 5.1 ± 0.1 dB, comparable to Si microring and hybrid-Si modulators [1–5]. For the 500 nm long device, the maximum ER was 4.0 dB. The

#228930 - $15.00 USD Received 4 Dec 2014; revised 20 Jan 2015; accepted 23 Jan 2015; published 5 Feb 2015
(C) 2015 OSA

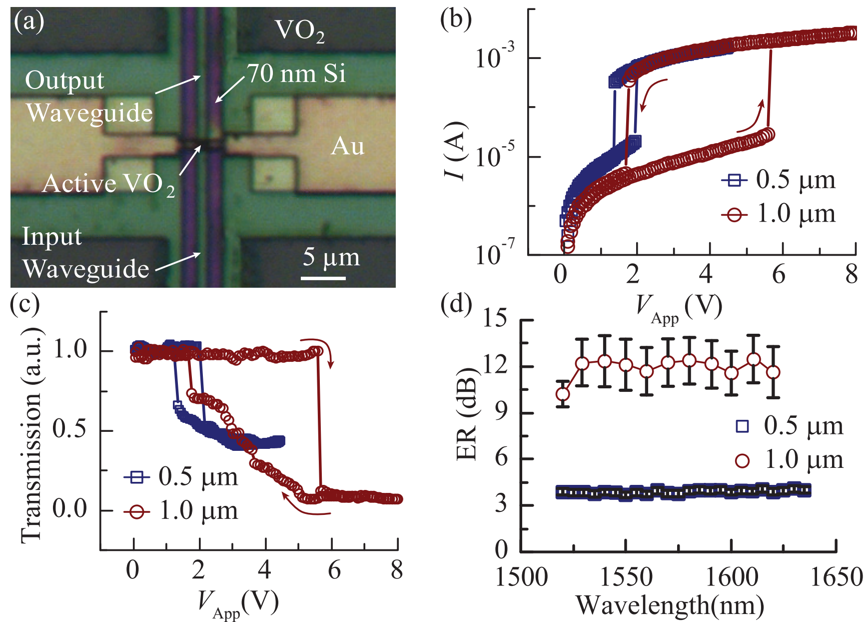

Fig. 3. (a) A microscope image of a device with a Si-VO_2 device length of 500 nm. The measured (b) current and (c) optical transmission as a function of the applied voltage. (d) The measured ER spectra for L_g of 500 nm and 1 μm.

lower ER-per-length was likely caused by variations in the VO_2 fil quality and adhesion on the Si waveguide. The ER spectrum is plotted in Fig. 3(d). The error bars represent the standard deviation in multiple ER measurements of a single device. The ER remained relatively constant over the wavelength range between 1520 nm and 1640 nm.

The discrepancy between the simulated and measured performance of the devices can be attributed to the difference in the refractive index of the VO_2 from values that were measured from planar VO_2 film on smooth Si substrates. Also, the adhesion of VO_2 to the partially etched Si surface was not strong after dry etching. Depositing a SiO_2 layer prior to VO_2 sputtering may improve the VO_2 adhesion and result in better VO_2 fil quality, a higher resistivity change across the phase transition, and a larger ER. Nonetheless, an ER >10 dB over a propagation length of 1 μm and ER > 4 dB for a 500 nm long device are, to the best of our knowledge, records in micron and sub-micron long integrated optical switches (e.g., compared to [26]).

The power consumption of the device can be determined from the dissipated electrical power as $P = IV_{\text{Gap}}$, where $V_{\text{Gap}} = V_{\text{App}} - IR_{\text{L}}$ and is the voltage across the VO_2. The device with $L_g = 500$ nm (1 μm) consumed 40 μW (150 μW) of power at the onset of the phase transition, and 650 μW (2.7 mW) when $V_{\text{App}} = 1.25V_{I\rightarrow M}$. The powers dissipated for the electroabsorption switching were about 610 μW and 2.55 mW for the 500 nm and 1 μm long devices, respectively. The power consumption is about an order of magnitude smaller than that of carrier injection Si variable optical attenuators [27, 28] and state-of-the-art Si thermo-optic switches [29]. The optical bandwidth of the hybrid Si-VO_2 switch is in excess of 12.5 THz, so the energy consumption for switching the throughput would be less than 0.2 fJ/bit. From measurements of VO_2 microwires and gap junctions, we believe that the contact resistance has a significan contribution to the power dissipation [19, 24]. The power consumption can be reduced by doping the VO_2 to reduce the interface contact resistance.

#228930 - $15.00 USD Received 4 Dec 2014; revised 20 Jan 2015; accepted 23 Jan 2015; published 5 Feb 2015
(C) 2015 OSA

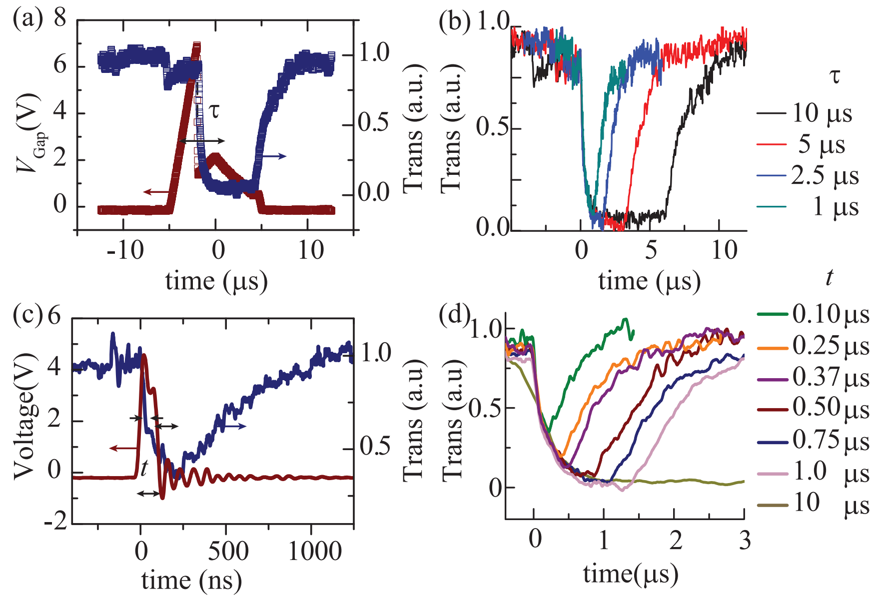

Fig. 4. (a) The measured voltage across the gap (left axis) and normalized optical transmission (right axis) when a triangular voltage pulse with a ramp-up time of τ was applied. (b) The optical transmission for several values of τ. (c) The measured voltage across the gap (left axis) and normalized optical transmission (right axis) when a square-wave pulse with a duration of t was applied. (d) The measured optical transmission for various values of t.

4.2. Switching dynamics

To investigate the switching dynamics of the 1 μm long device, we firs applied a periodic train of triangular voltage pulses with a ramp-up time of τ and a period of 1 s to avoid thermal accumulation from successive voltage pulses. Figure 4(a) shows the measured time profil of V_{Gap} (left axis), and the optical transmission of the device (right axis), when a triangular pulse with $\tau = 5$ μs was applied across the Au pads. At the onset of the phase transition, V_{Gap} and optical transmission dropped. The transmission remained at a minimum until the reverse phase transition voltage, at which point it increased to its original value. Since the reverse transition was dominated by thermal effects, the optical transmission was restored only when the heat was dissipated after the application of the voltage pulse. Figure 4(b) shows the time dependent optical transmission for various values of τ. The ER remained > 10 dB even when $\tau = 1$ μs, and the turn-on and turn-off rates of the switch did not change significantl with τ.

Next, to probe faster transients, we applied square-wave pulses with a duration of t and a period of 1 s. Figure 4(c) shows the temporal profile of V_{Gap} (left axis) and optical transmission (right axis) when $t = 150$ ns. The applied voltage pulse exhibited a decaying oscillation with a frequency of 14.3 MHz, which was an artifact of the setup. The phase transition was initiated about 50 ns after the start of the voltage pulse and caused a sharp drop in V_{Gap}. The optical transmission also reduced to about 60% of its initial value within the firs 50 ns, but continued to decrease after another 50 ns, as Joule heating raised the local VO_2 temperature. The transmission continued to decrease after the end of the voltage pulse and reached a minimum after 120 ns, after which the transmission gradually recovered its original value.

We separately fitte the fall and rise of the optical transmission to exponential functions and extracted a turn-off time constant of 350 ± 25 ns and turn-on time constant of 750 ± 20 ns

#228930 - $15.00 USD Received 4 Dec 2014; revised 20 Jan 2015; accepted 23 Jan 2015; published 5 Feb 2015
(C) 2015 OSA

(equivalent to an electro-optic bandwidth of about 1.3 MHz). Both time constants were limited by thermal dissipation. Owing to the small device size, the switching time constants were similar to that of commercially available carrier injection based Si optical attenuating switches [27] and much shorter than the microsecond time constants of Si thermo-optic switches [29] (as an aside, in Si, the carrier lifetime can be reduced to less than 10 ns at the expense of the attenuation efficien y [30]). The hybrid Si-VO_2 switch has a power-time constant ($P \cdot \tau$) product of about 0.9 mW $\cdot$ μs, about 10 times smaller than the Si attenuating switch in [27] and 20 times smaller than the Si thermo-optic switch in [29] for the same extinction ratio.

Figure 4(d) shows the optical transmission for several values of t. As expected, the ER was higher for larger values of t and saturated to the DC value when $t \geq 500$ ns. To improve the turn-on and turn-off time constants, R_L can be increased and the current can be regulated to suppress Joule heating and use only the electronically induced part of the phase transition at the expense of the ER-per-length [24]. If only the electronic transition of VO_2 is used, the switching time can be reduced to $\lesssim 50$ ns (the time-scale for the initial drop of the optical transmission in Fig. 4(c)) and the ER would be less than 2.0 ± 0.2 dB/μm [24, 31].

4.3. Performance limits of VO_2 electroabsorption switches and modulators

Based on the material properties of our VO_2 samples [24, 25], we can project some of the performance limits of VO_2 waveguide electroabsorption modulators and switches. Recent optical experiments have shown that injection of electrons can initiate the phase transition of VO_2 at (sub)picosecond timescales [32–34], which indicates that the phase transition can be inherently fast, making VO_2 promising for the development of high-speed modulators. Table 1 summarizes the estimated performance metrics. The VO_2 optical switch would operate by sweeping the voltage without any current clamping, which would initiate both the electronic and thermally induced parts of the phase transition [24, 25]. The modulator would operate by sweeping the current, which can selectively induce the electronic part of the phase transition for a fast operation speed [24, 25]. A regulated current suppresses the thermal effects that lead to the second, thermal step of the phase transition.

For the estimates, we have assumed the VO_2 device width is 1 μm, a maximum absorption change of 30 dB/μm, and a 100$\times$ change in the electrical resistivity. We have neglected any losses due to mode matching and electrical parasitics due to impedance mismatch. The power consumption is extrapolated from the measurements in [24, 25] based on the device dimension and ignoring the contact resistance. The modulation bandwidths are estimated from the theoretical thermal transport times [35] and ultrafast studies of the VO_2 phase transition [32–34]. If the VO_2 material (e.g., fil quality and uniformity) and contact resistance challenges are solved, VO_2 can become highly attractive for ultra- efficien and compact optical switches and modulators.

5. Photodetectors

The hybrid Si-VO_2 devices also have the potential to operate as highly sensitive photodetectors [36], though a more optimal waveguide design for photodetectors would completely couple the light into the VO_2 (i.e., no optical output would be necessary). Vanadium oxides are often used for bolometers which detect long infrared wavelengths. For shorter infrared wavelengths in the telecommunication window, optical absorption by VO_2 biased near the onset of the insulator-metal transition can generate the carriers to initiate the insulator-metal phase transition, which can also result in a giant responsivity. Even without initiating the phase transition, optically generated carriers in the VO_2 increase the absorption of light and can be extracted to achieve photodetector functionality. Figure 5(a) shows the optical transmission at $\lambda = 1550$ nm through the 1 μm long Si-VO_2 device without a bias voltage as the incident optical power was increased.

Table 1. Estimate of performance limits of VO_2 electroabsorption switches and modulators

	Switches	**Modulators**
Transition mechanism	Electronic+Thermal	Electronic
Device width	1 μm	1 μm
Device length	330 nm	2 μm [a]
Extinction ratio	10 dB	10 dB
Insertion loss	$\sim$ 1 dB	$\sim$ 6 dB
Optical bandwidth	$>$ 100 nm	$>$ 100 nm
Threshold current [b]	20 μA	20 μA
Static dissipated power [c]	$\sim$ 20 μW	$\sim$ 20 μW
Dynamic dissipated power	$\sim$ 2.4 mW [d]	$\sim$ 15 μW [e]
Modulation bandwidth	$\sim$ 0.1-1 GHz	$\sim$ 1-100 GHz
Energy consumption	$\sim$ 3 - 30 pJ/bit	$\sim$ 0.35 - 35 fJ/bit

[a] The change in absorption is reduced using only the electronic part of the phase transition.

[b] From [24].

[c] The power dissipated at the phase transition threshold. The threshold electric fiel is 12 kV/cm [24].

[d] Taken to be $\frac{1}{2}V|\Delta I|$, where ΔI is the current change across the phase transition.

[e] Taken to be $\frac{1}{2}I|\Delta V|$, where ΔV is the voltage change across the electronic part of the phase transition.

The incident power refers to the coupled optical power into the Si-VO_2 section, and it was estimated from a comparison between the transmission of the Si-VO_2 device test structure and the transmission of a reference waveguide without the Si-VO_2 section. The data was normalized to the optical transmission as the incident optical power approached 0 μW. As expected, the optical absorption reduced the transmission due to an increase in carrier density through either Joule heating or interband transitions.

Figure 5(b) shows examples of the resistance of the VO_2 wire, R_{Gap}, as a function of the applied voltage, V_{App}, at two incident optical powers. The change in the phase transition voltage, $\Delta V_{\text{I}\to\text{M}}$, and resistance just after the phase transition, ΔR_{Gap}, are marked on the plot. By measuring the dependence of $\Delta V_{\text{I}\to\text{M}}$ and ΔR_{Gap} on the incident optical power, we can quantify the photodetector response. Of these two parameters, however, the standard deviation in $\Delta V_{\text{I}\to\text{M}}$ over several measurements at a fi ed incident power was generally $> 25\%$ of $\Delta V_{\text{I}\to\text{M}}$; thus, $\Delta V_{\text{I}\to\text{M}}$ was not suitable for quantifying the photodetector response. The variations in $V_{\text{I}\to\text{M}}$ were likely due to competing current filamen paths with similar resistivities at the onset of the phase transition. Unlike $V_{\text{I}\to\text{M}}$, R_{Gap}, which only depended on the metallic phase characteristics of VO_2, was consistent over several measurements. Our measurements showed that R_{Gap} had a standard deviation which was only 0.5% of ΔR_{Gap}.

Because we found it difficul to stably and repeatably bias the device at the onset of the transition, for the experimental results to follow, we biased the device just above the insulator-metal transition voltage at 5.8 V. Active feedback of the bias voltage would likely be necessary to maintain the bias of the hybrid Si-VO_2 photodetector for maximum sensitivity. Nonetheless, at a fi ed bias voltage above the transition voltage, the change of ΔR_{Gap} as a function of the input optical power translates to an optical power dependent current through the device. Figure 5(c) shows the measured (symbols) change in the current through the device as a function of the input optical power. Two regimes of operation could be identifie and are marked with the green and blue fittin lines. At low optical powers, the change in the current increased with the incident power and saturated at about 10 μW; at high optical powers around 100 μW, a much larger current change was observed.

The difference in the change in current can be explained by the mechanisms behind the

#228930 - $15.00 USD Received 4 Dec 2014; revised 20 Jan 2015; accepted 23 Jan 2015; published 5 Feb 2015
(C) 2015 OSA

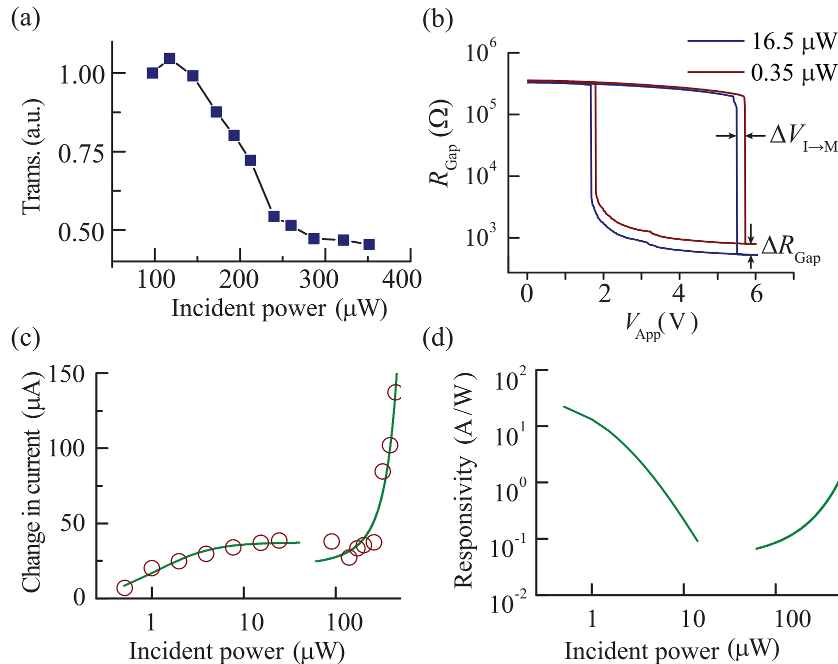

Fig. 5. (a) The normalized optical transmission through the 1 μm long Si-VO_2 device as a function of the incident optical power coupled into the Si-VO_2 section. (b) The measured device resistance as a function of applied voltage for incident optical powers of 0.35 μW and 16.5 μW. (c) The measured (circles) and fitte (solid lines) change in the current through the device when a bias voltage of 5.8 V was applied. The curve on the left is a fi of the form $A/(P_o - B)^2 + C$, where P_o is the incident optical power, and the curve on the right is an exponential fit (d) The extracted responsivity of the 1 μm long photodetector.

photodetection. At low optical incident powers up to about 10 μW, the VO_2 grains close to the phase transition threshold were switched to the metallic phase via optical absorption. When most of the grains transitioned to the metallic phase, the absorption of light would not further increase the current, resulting in the saturation near 10 μW. We phenomenologically fitte the data at low powers using a function of the form $A/(P_o - B)^2 + C$, where P_o is the incident optical power in μW, and $A = -200$ μAμW^2, $B = 1.0$ μW and $C = 37.0$ μA are fittin parameters. Above 100 μW, the absorption of optical power resulted in a nearly exponential increase in the current due to the Joule heating of VO_2 through optical absorption of light with lowered the resistivity of the VO_2. The solid line in the right half of Fig. 5(c) shows an exponential fi of the form $D\exp(P_o/E) + F$, where $D = 35$ μA, $E = 310$ μW, and $F = 14.5$ μA are the fittin parameters.

From the derivative of the fits we extracted the effective responsivity of the Si-VO_2 photodetectors as shown in Fig. 5(d). At low incident powers, the responsivity was well above 10 A/W due to the optical absorption by VO_2 grains. At high optical powers, this responsivity decreased to about 0.5 A/W due to the Joule heating of VO_2. The detection limit of the mode of device operation described here is set by the fluctuation in R_{Gap} at a bias of 5.8 V, which resulted in an effective "dark current" of 1 μA. This "dark current" would theoretically lead to a maximum responsivity of 30 A/W or a detection limit of 30 nW of optical power. The fundamental upper-bound of the responsitvity of a photodetector relying on band-to-band transition for a wavelength of 1550 nm is about 1.25 A/W. The ultimate performance limits of a VO_2

photodetector are difficul to estimate from our measurements, as the performance limits would be determined by the noise spectral density which we have not determined. Nonetheless, the hybrid Si-VO_2 phase-transition photodetector shown here has a multiplicative factor of about 10, similar to avalanche photodiodes, demonstrating the promise of VO_2 for highly sensitive optical detection in the near infrared wavelength range.

6. Conclusion

We have demonstrated wavelength-size, broadband hybrid Si-VO_2 electroabsorption optical switches with a record per-length extinction ratio and competitive insertion losses as for wavelengths near 1550 nm. We also showed that the same devices can be used as efficien photodetectors. The volumes of these devices are smaller than today's Si and hybrid-Si devices by about 2 to 3 orders of magnitude. As an optical switch, the small volumes resulted in thermally-limited switching time constants similar to carrier injection Si attenuating switches and a greater than 10-fold reduction in power consumption. The switching time constants can be improved at the cost of a reduced ER by using only the electronic (and not thermal) part of the VO_2 phase transition. The thermal dissipation rate can also be improved, for example, by reducing contact resistance, which would also increase the modulation bandwidth. Eliminating Joule heating would reduce the switching time constant of our VO_2 samples with integrated electrical contacts to roughly 50 ns, so their bandwidths may become closer to that of Si modulators. Today's carrier depletion Si modulators have device footprints ranging from about 10^2 μm^2 to 10^4 μm^2, but can have GHz modulation bandwidths (see, for example, [2, 37, 38]). In photodetection mode, we showed the devices can have high responsivities, similar to avalanche photodiodes, at low input optical powers. The responsivity of the hybrid Si-VO_2 photodetector can be orders of magnitude higher if the device can be stably biased near or at the onset of the phase transition. The results presented here demonstrate the potential of VO_2 and transition metal oxides for fully integrated nanoscale optical modulators and photodetectors.

Acknowledgment

The financia support of the Ontario Graduate Scholarship program, Natural Sciences and Engineering Research Council of Canada, and Canada Research Chairs program is gratefully acknowledged. The micro- and nano-fabrication was completed at the Toronto Nanofabrication Centre at the University of Toronto.